Tuovinen, Toni; Awan, Hafiz Asad Ali; Kukkola, Jarno; Saarakkala, Seppo E.; Hinkkanen, Marko

Permanent-magnet flux adaptation for sensorless synchronous motor drives

Published in:
IEEE 9th International Symposium on Sensorless Control for Electrical Drives, SLED 2018

DOI:
10.1109/SLED.2018.8485899

Published: 13/09/2018

Document Version
Peer-reviewed accepted author manuscript, also known as Final accepted manuscript or Post-print

Please cite the original version:
Tuovinen, T., Awan, H. A. A., Kukkola, J., Saarakkala, S. E., & Hinkkanen, M. (2018). Permanent-magnet flux adaptation for sensorless synchronous motor drives. In *IEEE 9th International Symposium on Sensorless Control for Electrical Drives, SLED 2018* (pp. 138-143). (IEEE international symposium on sensorless control for electrical drives). IEEE. https://doi.org/10.1109/SLED.2018.8485899

Permanent-Magnet Flux Adaptation for Sensorless Synchronous Motor Drives

Toni Tuovinen*, Hafiz Asad Ali Awan†, Jarno Kukkola*, Seppo E. Saarakkala†, and Marko Hinkkanen†
*ABB Drives, Helsinki, Finland
†Aalto University School of Electrical Engineering, Espoo, Finland

***Abstract*—This paper deals with estimation of the permanent-magnet (PM) flux in sensorless synchronous motor drives. A back-electromotive-force (back-EMF)-based observer is augmented with an adaptation law for the PM flux magnitude. The gains of the augmented observer are designed based on the linearized model. The proposed design makes PM flux estimation independent of speed estimation and enables straightforward analytical pole placement of the observer. Practical design guidelines are given. The proposed design is evaluated by means of simulations and laboratory experiments using a 2.2-kW interior PM synchronous motor drive.**

***Index Terms*—Observer, parameter adaptation, permanent magnet (PM), speed sensorless, stability conditions.**

I. Introduction

Sensorless control is a relevant technology in permanent-magnet (PM) synchronous motor drives. As an example, removing the need for a fragile motion sensor makes it possible to reduce the overall size and to improve reliability in traction drives. Rotor-position estimation for sensorless control is typically realized using a back-electromotive-force (back-EMF)-based observer [1]–[4], augmented with a signal-injection method for operation at lowest speeds.

At low speeds, the back-EMF-based observers are sensitive to errors in the stator resistance. As the speed and the back-EMF increase, position estimation becomes more sensitive to errors in the magnetic model parameters. The inductances (or saturation characteristics) can be identified during the self-commissioning stage without rotating the shaft [5], [6]. On the other hand, the PM flux cannot be properly estimated without spinning the rotor. If the application allows only standstill commissioning, a rough estimate for the PM flux can be computed based on the motor nameplate data. The PM flux also changes with temperature [7]–[9]. Inaccuracies in the PM-flux estimate result in decreased control performance, position estimation errors, and even instability [10].

To increase the accuracy of the PM-flux estimate, online identification and adaptation schemes have been proposed [8], [11]–[14]. In [14], the back-EMF-based observer is augmented with a parameter adaptation law for the PM flux. Moreover, the PM flux is estimated from the d-direction current estimation error with an integral adaptation law while the speed is obtained from the q-direction estimation error [14].

In this paper, a back-EMF-based observer augmented with a PM-flux adaptation law is considered. The main contributions are:

1) The PM-flux adaptation law considered in [14] is modified in such a way that PM-flux estimation can be designed independently of speed estimation. This modification simplifies the observer design and eliminates undesired transients from the PM-flux estimate.
2) Analytical expressions for the gains of the augmented observer are developed in a form, which allows placing the closed-loop poles of the linearized estimation-error dynamics.
3) Practical design guidelines are given for the free design parameters of the augmented observer.

The observer design is evaluated by means of simulations and laboratory experiments using a 2.2-kW interior PM synchronous motor drive.

II. Motor Model

Real space vectors are used. Vectors are denoted using boldface lowercase letters and matrices using boldface uppercase letters. For example, the current vector is $\boldsymbol{i} = [i_\mathrm{d}, i_\mathrm{q}]^\mathrm{T}$, where i_d and i_q are the components of the vector. The identity matrix is $\mathbf{I} = \left[\begin{smallmatrix} 1 & 0 \\ 0 & 1 \end{smallmatrix}\right]$ and the orthogonal rotation matrix is $\mathbf{J} = \left[\begin{smallmatrix} 0 & -1 \\ 1 & 0 \end{smallmatrix}\right]$.

The electrical rotor angle is ϑ_m and the electrical angular rotor speed is $\omega_\mathrm{m} = \mathrm{d}\vartheta_\mathrm{m}/\mathrm{d}t$. The electrical radians are used throughout the paper. In rotor coordinates, the inductance matrix and the PM-flux linkage vector, respectively, are denoted by

$$\boldsymbol{L} = \begin{bmatrix} L_\mathrm{d} & 0 \\ 0 & L_\mathrm{q} \end{bmatrix} \qquad \boldsymbol{\psi}_\mathrm{f} = \begin{bmatrix} \psi_\mathrm{f} \\ 0 \end{bmatrix} \tag{1}$$

where L_d is the direct-axis inductance, L_q is the quadrature-axis inductance, and ψ_f is the PM flux. The machine model is expressed in *estimated* rotor coordinates, whose d-axis is aligned at $\hat{\vartheta}_\mathrm{m}$ with respect to the stator coordinates. The stator flux linkage is

$$\boldsymbol{\psi} = \boldsymbol{L}'\boldsymbol{i} + \boldsymbol{\psi}'_\mathrm{f} \tag{2}$$

where the inductance matrix and PM-flux vector, respectively,

$$\boldsymbol{L}' = \mathrm{e}^{\tilde{\vartheta}_\mathrm{m}\mathbf{J}}\boldsymbol{L}\,\mathrm{e}^{-\tilde{\vartheta}_\mathrm{m}\mathbf{J}} \qquad \boldsymbol{\psi}'_\mathrm{f} = \mathrm{e}^{\tilde{\vartheta}_\mathrm{m}\mathbf{J}}\boldsymbol{\psi}_\mathrm{f} \tag{3}$$

depend nonlinearly on the estimation error $\tilde{\vartheta}_\mathrm{m} = \vartheta_\mathrm{m} - \hat{\vartheta}_\mathrm{m}$ of the rotor position. The stator voltage is

$$\boldsymbol{u} = R\boldsymbol{i} + \frac{\mathrm{d}\boldsymbol{\psi}}{\mathrm{d}t} + \hat{\omega}_\mathrm{m}\mathbf{J}\boldsymbol{\psi} \tag{4}$$

where R is the resistance and $\hat{\omega}_\mathrm{m} = \mathrm{d}\hat{\vartheta}_\mathrm{m}/\mathrm{d}t$ is the angular speed of the coordinate system.

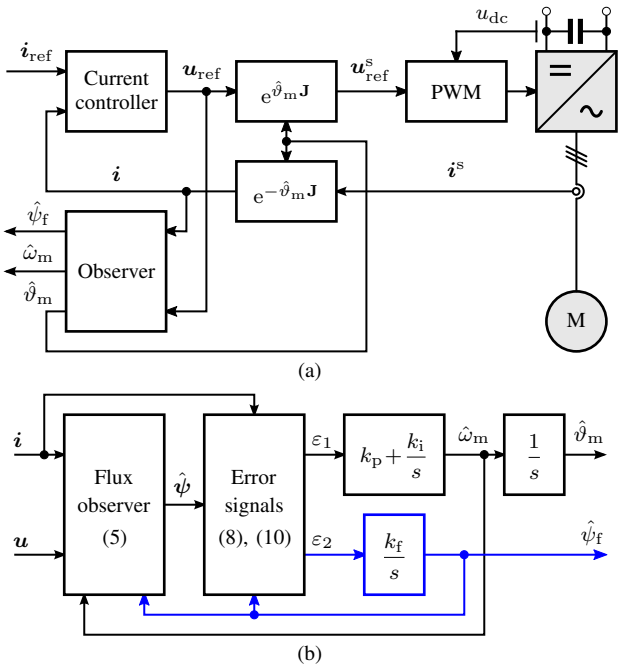

Fig. 1. (a) Block diagram of the sensorless control system. The DC-link voltage u_{dc} and the phase currents are measured. The deadtime effect and power device voltage drops are compensated for in the pulse-width modulator (PWM) using the phase-current feedback. Space vectors in stator coordinates are marked with the superscript s. (b) Internal structure of the observer. The blue lines and blocks represent PM-flux adaptation.

III. Observer

A. Structure

Fig. 1(a) shows the overall structure of the sensorless control scheme. Fig. 1(b) shows the internal structure of the observer, operating in estimated rotor coordinates. The flux observer is defined by [4]

$$\frac{\mathrm{d}\hat{\boldsymbol{\psi}}}{\mathrm{d}t} = \boldsymbol{u} - R\boldsymbol{i} - \hat{\omega}_{\mathrm{m}}\mathbf{J}\hat{\boldsymbol{\psi}} + \boldsymbol{K}\boldsymbol{e} \tag{5a}$$

$$\boldsymbol{e} = \boldsymbol{L}\boldsymbol{i} + \hat{\boldsymbol{\psi}}_{\mathrm{f}} - \hat{\boldsymbol{\psi}} \tag{5b}$$

where $\boldsymbol{K}$ is a 2×2 observer gain matrix, the estimated PM-flux vector is $\hat{\boldsymbol{\psi}}_{\mathrm{f}} = [\hat{\psi}_{\mathrm{f}}, 0]^{\mathrm{T}}$, and estimates are marked with a hat. The correction vector $\boldsymbol{e}$ is equal to the difference between the measured current and the estimated current, scaled by the inductance matrix.

As shown in Fig. 1(b), the proportional-integral (PI) mechanism is used to drive the error signal ε_1 to zero by adjusting the speed estimate

$$\frac{\mathrm{d}\hat{\omega}_{\mathrm{mi}}}{\mathrm{d}t} = \varepsilon_1 \tag{6a}$$

$$\hat{\omega}_{\mathrm{m}} = k_{\mathrm{p}}\varepsilon_1 + k_{\mathrm{i}}\hat{\omega}_{\mathrm{mi}} \tag{6b}$$

where k_{p} and k_{i} are the gains and $\hat{\omega}_{\mathrm{mi}}$ is the integral state. The speed estimate is further fed to the integrator for getting the position estimate as

$$\frac{\mathrm{d}\hat{\vartheta}_{\mathrm{m}}}{\mathrm{d}t} = \hat{\omega}_{\mathrm{m}} \tag{7}$$

The error signal used in (6) is defined by means of the scalar product

$$\varepsilon_1 = \boldsymbol{\lambda}^{\mathrm{T}}\mathbf{J}\boldsymbol{e} \tag{8}$$

where the projection vector $\boldsymbol{\lambda}$ can be a constant vector or it may depend on $\hat{\boldsymbol{\psi}}$ and $\boldsymbol{i}$.

The PM flux is adapted using the integral mechanism

$$\frac{\mathrm{d}\hat{\psi}_{\mathrm{f}}}{\mathrm{d}t} = k_{\mathrm{f}}\varepsilon_2 \tag{9}$$

where k_{f} is the adaptation gain and the error signal is

$$\varepsilon_2 = \boldsymbol{\lambda}^{\mathrm{T}}\boldsymbol{e} \tag{10}$$

As can be noticed from (8) and (10), the orthogonal components of the correction signal $\boldsymbol{e}$ are used to calculate the error signals ε_1 and ε_2. Furthermore, the magnitude of the projection vector $\boldsymbol{\lambda}$ is irrelevant due to the adaptation gains, while its direction affects the properties of the observer.

B. Linearized Estimation-Error Dynamics

The nonlinear estimation-error dynamics can be linearized for analysis purposes, as explained in [14], [15]. The operating-point quantities are marked with the subscript 0. The accurate model parameters are assumed, making the operating-point estimation errors zero, e.g., $\hat{\vartheta}_{\mathrm{m0}} = \vartheta_{\mathrm{m0}}$, further leading to $\boldsymbol{L}'_0 = \boldsymbol{L}$ and $\boldsymbol{\psi}'_{\mathrm{f0}} = \hat{\boldsymbol{\psi}}_{\mathrm{f0}} = \boldsymbol{\psi}_{\mathrm{f}}$. The standard linearization procedure of (2)–(10) gives a state-space representation

$$\frac{\mathrm{d}\boldsymbol{x}}{\mathrm{d}t} = \boldsymbol{A}\boldsymbol{x} + \boldsymbol{B}_1\omega_{\mathrm{m}} + \boldsymbol{B}_2\psi_{\mathrm{f}} \tag{11a}$$

$$\hat{\omega}_{\mathrm{m}} = \boldsymbol{C}_1\boldsymbol{x} + D_1\psi_{\mathrm{f}} \tag{11b}$$

$$\hat{\psi}_{\mathrm{f}} = \boldsymbol{C}_2\boldsymbol{x} \tag{11c}$$

where the state vector and system matrices are

$$\boldsymbol{x} = \begin{bmatrix} \tilde{\boldsymbol{\psi}} \\ \hat{\psi}_{\mathrm{f}} \\ \hat{\omega}_{\mathrm{mi}} \\ \tilde{\vartheta}_{\mathrm{m}} \end{bmatrix} \qquad \boldsymbol{B}_1 = \begin{bmatrix} \mathbf{0} \\ 0 \\ 0 \\ 1 \end{bmatrix} \qquad \boldsymbol{B}_2 = \begin{bmatrix} \boldsymbol{k}_0 \\ -k_{\mathrm{f}}\lambda_{\mathrm{d0}} \\ -\lambda_{\mathrm{q0}} \\ k_{\mathrm{p}}\lambda_{\mathrm{q0}} \end{bmatrix}$$

$$\boldsymbol{A} = \begin{bmatrix} -\boldsymbol{K}_0 - \omega_{\mathrm{m0}}\mathbf{J} & -\boldsymbol{k}_0 & \mathbf{0} & \boldsymbol{K}_0\mathbf{J}\boldsymbol{\psi}_{\mathrm{a0}} \\ k_{\mathrm{f}}\boldsymbol{\lambda}_0^{\mathrm{T}} & k_{\mathrm{f}}\lambda_{\mathrm{d0}} & 0 & -k_{\mathrm{f}}\boldsymbol{\lambda}_0^{\mathrm{T}}\mathbf{J}\boldsymbol{\psi}_{\mathrm{a0}} \\ \boldsymbol{\lambda}_0^{\mathrm{T}}\mathbf{J} & \lambda_{\mathrm{q0}} & 0 & \boldsymbol{\lambda}_0^{\mathrm{T}}\boldsymbol{\psi}_{\mathrm{a0}} \\ -k_{\mathrm{p}}\boldsymbol{\lambda}_0^{\mathrm{T}}\mathbf{J} & -k_{\mathrm{p}}\lambda_{\mathrm{q0}} & -k_{\mathrm{i}} & k_{\mathrm{p}}\boldsymbol{\lambda}_0^{\mathrm{T}}\boldsymbol{\psi}_{\mathrm{a0}} \end{bmatrix}$$

$$\boldsymbol{C}_1 = \begin{bmatrix} k_{\mathrm{p}}\boldsymbol{\lambda}_0^{\mathrm{T}}\mathbf{J} & k_{\mathrm{p}}\lambda_{\mathrm{q0}} & k_{\mathrm{i}} & -k_{\mathrm{p}}\boldsymbol{\lambda}_0^{\mathrm{T}}\boldsymbol{\psi}_{\mathrm{a0}} \end{bmatrix}$$

$$\boldsymbol{C}_2 = \begin{bmatrix} \mathbf{0} & 1 & 0 & 0 \end{bmatrix} \qquad D_1 = k_{\mathrm{p}}\lambda_{\mathrm{q0}} \tag{12}$$

and $\tilde{\boldsymbol{\psi}} = \boldsymbol{\psi} - \hat{\boldsymbol{\psi}}$ is the flux estimation error. Furthermore, in order to simplify the notation, an auxiliary flux linkage vector is defined as

$$\begin{aligned} \boldsymbol{\psi}_{\mathrm{a0}} &= (\boldsymbol{L} + \mathbf{J}\boldsymbol{L}\mathbf{J})\boldsymbol{i}_0 + \boldsymbol{\psi}_{\mathrm{f}} \\ &= \begin{bmatrix} (L_{\mathrm{d}} - L_{\mathrm{q}})i_{\mathrm{d0}} + \psi_{\mathrm{f}} \\ -(L_{\mathrm{d}} - L_{\mathrm{q}})i_{\mathrm{q0}} \end{bmatrix} = \begin{bmatrix} \psi_{\mathrm{ad0}} \\ \psi_{\mathrm{aq0}} \end{bmatrix} \end{aligned} \tag{13}$$

and the gains are given by

$$\boldsymbol{k}_0 = \boldsymbol{K}_0 \begin{bmatrix} 1 \\ 0 \end{bmatrix} \qquad \boldsymbol{\lambda}_0 = \begin{bmatrix} \lambda_{\mathrm{d0}} \\ \lambda_{\mathrm{q0}} \end{bmatrix} \tag{14}$$

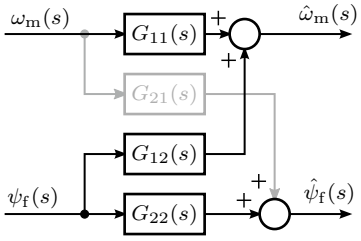

Fig. 2. Linearized model of the estimation-error dynamics.

The properties of (11) depend on the observer gain $\boldsymbol{K}_0$, the projection vector $\boldsymbol{\lambda}_0$, the speed-adaptation gains k_p and k_i, and the PM-flux adaptation gain k_f.

Fig. 2 shows the block diagram corresponding to the linearized model. The transfer functions are obtained from (11). As examples, the transfer function from the actual speed $\omega_\mathrm{m}(s)$ to the estimated speed $\hat{\omega}_\mathrm{m}(s)$ is

$$G_{11}(s) = \frac{\hat{\omega}_\mathrm{m}(s)}{\omega_\mathrm{m}(s)} = \boldsymbol{C}_1(s\mathbf{I} - \boldsymbol{A})^{-1}\boldsymbol{B}_1 \tag{15}$$

and the transfer function from the actual PM-flux $\psi_\mathrm{f}(s)$ to the PM-flux estimate $\hat{\psi}_\mathrm{f}(s)$ is

$$G_{22}(s) = \frac{\hat{\psi}_\mathrm{f}(s)}{\psi_\mathrm{f}(s)} = \boldsymbol{C}_2(s\mathbf{I} - \boldsymbol{A})^{-1}\boldsymbol{B}_2 \tag{16}$$

The closed-form expressions for these transfer functions can be easily calculated using any symbolic mathematics package.

IV. Proposed Gains and Design Guidelines

A. Proposed Gain Selection

A gain selection for the observer with PM-flux adaptation is proposed. The analysis is based on the linearized model (11), which is of the fifth order and has two inputs and two outputs. To ease the gain selection, the dynamics of this system are to be splitted and to be partly decoupled.

Based on the system matrix $\boldsymbol{A}$ in (12), the speed-adaptation loop can be decoupled from the flux observer and from the PM-flux adaptation loop if the following conditions are fulfilled

$$\boldsymbol{K}_0\mathbf{J}\boldsymbol{\psi}_\mathrm{a0} = \mathbf{0} \qquad \boldsymbol{\lambda}_0^\mathrm{T}\mathbf{J}\boldsymbol{\psi}_\mathrm{a0} = 0 \tag{17}$$

resulting in $G_{21}(s) = 0$ in Fig. 2. The latter condition can be met simply by choosing a suitable projection vector

$$\boldsymbol{\lambda}_0 = \frac{\boldsymbol{\psi}_\mathrm{a0}}{\|\boldsymbol{\psi}_\mathrm{a0}\|^2} \tag{18}$$

Only the direction of the vector $\boldsymbol{\lambda}_0$ is relevant, while the magnitude of $\boldsymbol{\lambda}_0$ is chosen to simplify the following expressions. It is also worth noticing that the projection vector $\boldsymbol{\lambda}_0 = [\lambda_\mathrm{d0}, 0]^\mathrm{T}$, which is often applied for speed estimation [14], [15], does not fulfil the latter condition in (17).

1) Flux Observer: The first condition in (17) is also met, if the observer gain matrix is selected as [4], [16]

$$\boldsymbol{K} = \begin{bmatrix} k_1' \\ k_2' \end{bmatrix} \frac{\boldsymbol{\psi}_\mathrm{a0}^\mathrm{T}}{\psi_\mathrm{ad0}} = \begin{bmatrix} k_1' & -\beta k_1' \\ k_2' & -\beta k_2' \end{bmatrix} \tag{19}$$

where k_1' and k_2' are free parameters and β is an auxiliary variable given by

$$\beta = -\frac{\psi_\mathrm{aq0}}{\psi_\mathrm{ad0}} = \frac{(L_\mathrm{d} - L_\mathrm{q})i_\mathrm{q0}}{\psi_\mathrm{f} + (L_\mathrm{d} - L_\mathrm{q})i_\mathrm{d0}} \tag{20}$$

The division by ψ_ad0 in (19) is introduced in order to simplify the following equations only.

For pole placement purposes, the parameters k_1' and k_2' are selected as

$$k_1' = -k_1 + \frac{k_2 a}{\omega_\mathrm{m0}} \qquad k_2' = -k_2 - \frac{k_1 a}{\omega_\mathrm{m0}} \tag{21}$$

where the coefficient $a \geq 0$ is related to the pole location of PM-flux adaptation. The gains k_1 and k_2 are given by

$$k_1 = -\frac{b + \beta(c/\omega_\mathrm{m0} - \omega_\mathrm{m0})}{\beta^2 + 1} \qquad k_2 = \frac{\beta b - c/\omega_\mathrm{m0} + \omega_\mathrm{m0}}{\beta^2 + 1} \tag{22}$$

where the coefficients $b \geq 0$ and $c \geq 0$ are related to the pole locations of the flux observer. If the PM-flux adaptation bandwidth is zero ($a = 0$), the observer gain reduces to the gain in [4], [16], where no PM-flux adaptation is used.

2) Speed Adaptation: Under the proposed gain selection, the transfer function (15) from the actual speed to the speed estimate reduces to

$$\begin{aligned} \frac{\hat{\omega}_\mathrm{m}(s)}{\omega_\mathrm{m}(s)} &= \frac{(s+a)(s^2+bs+c)(sk_\mathrm{p}+k_\mathrm{i})}{(s+a)(s^2+bs+c)(s^2+sk_\mathrm{p}+k_\mathrm{i})} \\ &= \frac{sk_\mathrm{p}+k_\mathrm{i}}{s^2+sk_\mathrm{p}+k_\mathrm{i}} \end{aligned} \tag{23}$$

where the speed-adaptation gains $k_\mathrm{p} > 0$ and $k_\mathrm{i} > 0$ are now directly the coefficients of the characteristic polynomial. Even if the flux-observer dynamics and the PM-flux adaptation dynamics cancel out from (23), they still are a part of the whole system and the corresponding closed-loop poles should be properly placed.

3) PM-Flux Adaptation: If the PM-flux adaptation gain is

$$k_\mathrm{f} = -\frac{ac}{\lambda_\mathrm{d0}\omega_\mathrm{m0}^2} \tag{24}$$

the transfer function (16) reduces to

$$\begin{aligned} \frac{\hat{\psi}_\mathrm{f}(s)}{\psi_\mathrm{f}(s)} &= \frac{(ac/\omega_\mathrm{m0}^2)(s^2+\omega_\mathrm{m0}^2)(s^2+sk_\mathrm{p}+k_\mathrm{i})}{(s+a)(s^2+bs+c)(s^2+sk_\mathrm{p}+k_\mathrm{i})} \\ &= \frac{(c/\omega_\mathrm{m0}^2)(s^2+\omega_\mathrm{m0}^2)}{s^2+bs+c}\frac{a}{s+a} \end{aligned} \tag{25}$$

It can be noticed that because the conditions in (17) are met, the speed-adaptation loop does not affect the operation of the PM-flux adaptation loop. This decoupling feature simplifies the design procedure of the observer, since PM-flux adaptation can be designed independently of speed adaptation. However, the coupling between the flux observer and the PM-flux adaptation loop still exists.

TABLE I
DATA OF A 2.2-KW INTERIOR PM SYNCHRONOUS MOTOR

Parameter	Value	Value (p.u.)
Rating		
Voltage (phase-neutral, peak)	$\sqrt{2/3} \cdot 370$ V	1
Current (peak)	$\sqrt{2} \cdot 4.3$ A	1
Frequency	75 Hz	1
Speed	1 500 r/min	1
Torque	14 Nm	0.80
Model		
Resistance R	4.75 Ω	0.095
d-axis inductance L_d	36 mH	0.34
q-axis inductance L_q	51 mH	0.48
PM flux ψ_f	0.57 Vs	0.89

B. Design Guidelines

1) Flux Observer: In the following, some design guidelines for the observer with PM-flux adaptation are given. In order to keep the observer gain (19) within reasonable limits, the design parameters b and c should be selected such that the closed-loop poles of the flux observer remain in the vicinity of the open-loop system poles, which can be solved from $\det(s\mathbf{I} - R\boldsymbol{L}^{-1} - \omega_{\mathrm{m}0}\mathbf{J}) = 0$. The damping of the open-loop poles decreases as the speed increases [4]. In the closed-loop system, it is favorable to increase the damping of the poles at higher speeds. This condition can be achieved, e.g., by selecting the design parameters as follows [16]

$$b = b' + 0.75|\hat{\omega}_\mathrm{m}| \qquad c = 1.5b|\hat{\omega}_\mathrm{m}| \tag{26}$$

At zero speed, the flux-observer poles are placed at $s = 0$ and $s = -b'$. It is recommended to choose the constant b' larger than R/L_d and R/L_q [4].

2) Speed Adaptation: The two poles related to the speed-adaptation loop can be placed at $s = -\omega_\mathrm{o}$, i.e,

$$k_\mathrm{p} = \omega_\mathrm{o} \qquad k_\mathrm{i} = \omega_\mathrm{o}^2 \tag{27}$$

where ω_o can be considered as an approximate speed-adaptation bandwidth. It is favourable to select the bandwidth of the speed-adaptation loop to be at least $20 \ldots 30$ times higher than the bandwidth of the speed-control loop.

3) PM-Flux Adaptation: The actual PM-flux magnitude changes slowly as a function of the temperature. The PM-flux adaptation dynamics (25) are governed by the flux-observer poles, the pole at $s = -a$, and the zeros at $s = \pm \mathrm{j}\omega_{\mathrm{m}0}$. Due to these speed-dependent dynamics, it is advisable to enable PM-flux adaptation only at medium and higher speeds, e.g., at $|\hat{\omega}_\mathrm{m}| > 0.25$ p.u. Furthermore, the parameter a should have a lower value (e.g., $a = 0.1$ p.u.) in order to make the pole at $s = -a$ to dominate the PM-flux adaptation dynamics,

$$\frac{\hat{\psi}_\mathrm{f}(s)}{\psi_\mathrm{f}(s)} \approx \frac{a}{s + a} \tag{28}$$

Higher values for a could also be selected, but then a does not anymore represent the approximate bandwidth of the PM-flux adaptation loop.

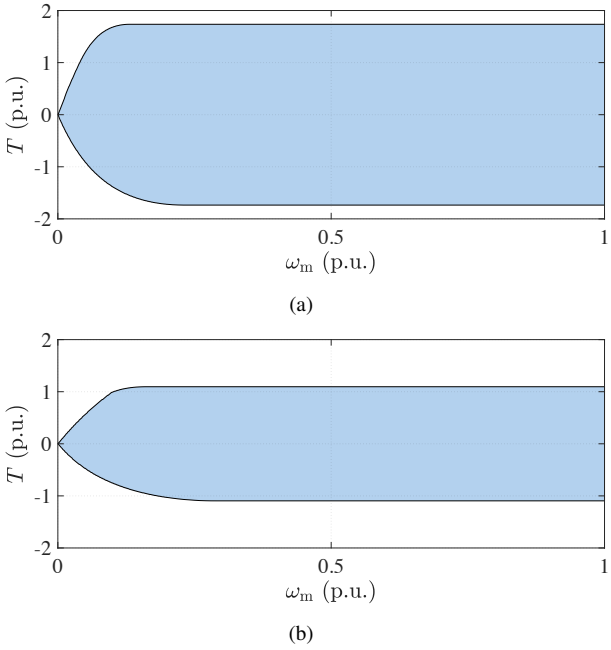

Fig. 3. Areas of stable operation (marked with blue color) in the space of the angular speed ω_m and actual torque T. The relative parameter uncertainty in parameter estimates L_d, L_q, and R is: (a) 25%; (b) 50%. The stable operation areas are limited due to the $i_{\mathrm{d,ref}} = 0$ control principle. With the MTPA control principle, the corresponding stable areas would be larger.

V. ROBUSTNESS ANALYSIS

The effect of the parameter errors on the local stability of the estimation-error dynamics is analyzed via the linearized model. The stability analysis can be carried out as follows. First, the erroneous values of the inductances and the stator resistance are inserted in the observer equation (5) and in the auxiliary flux linkage vector (13). The actual (correct) motor parameters are inserted in (1). Then, the steady-state operating point (i.e. $\tilde{\boldsymbol{\psi}}_0$ and $\tilde{\vartheta}_{\mathrm{m}0}$) is solved from (1)–(5) by assuming $\mathrm{d}\boldsymbol{\psi}/\mathrm{d}t = \mathrm{d}\hat{\boldsymbol{\psi}}/\mathrm{d}t = \boldsymbol{e} = \mathbf{0}$. Finally, the nonlinear model (2)–(10) is linearized in the vicinity of the given operating point in a similar manner as (11), taking into account the effects of the parameter errors. If the steady-state operating point does not exist or if any of the five eigenvalues of the linearized system matrix has a positive real part, the observer is considered unstable. Otherwise, the observer is considered stable.

In the following examples, the parameters of a 2.2-kW six-pole interior PM given in Table I are used. The design parameters are: $b' = 2\pi \cdot 20$ rad/s, $\omega_\mathrm{o} = 2\pi \cdot 100$ rad/s, and $a = 2\pi \cdot 7.5$ rad/s. For the sake of simplicity, the $i_{\mathrm{d,ref}} = 0$ control principle is applied. Fig. 3 shows areas of stable operation in the space of the angular speed and actual torque with erroneous model parameters. The relative parameter uncertainty is 25% in Fig. 3(a) and 50% in Fig. 3(b). The same relative uncertainty is assumed in all the parameter estimates at every speed-torque point and only the worst case is illustrated.

It can be noticed that slightly higher torque can be obtained

in the motoring mode than in the regenerating mode. For example, if the parameter uncertainty is 25%, the motoring torque of 1 p.u. can be reached at $\omega_{\mathrm{m0}} > 0.04$ p.u. If the parameter uncertainty is 50%, the motoring torque of 1 p.u. can be obtained at $\omega_{\mathrm{m0}} > 0.10$ p.u. However, this analysis does not include any errors there might be in the output voltage. With exact parameter estimates, any torque value could be reached, except at zero speed, where the observer is only marginally stable. The maximum available torque in this study is strongly limited due to the $i_{\mathrm{d,ref}} = 0$ control principle. This makes the system very sensitive to overestimation of L_{q}. If the maximum torque-per-ampere (MTPA) control principle is applied, the stable operation areas in Fig. 3 would clearly increase.

VI. Results

A. Implementation of a Control System

The motion-sensorless control system with PM-flux adaptation is evaluated by means of simulations and experiments using the 2.2-kW interior PM synchronous motor drive. The parameters of the motor are given in Table I. A sensorless control system was implemented on a dSPACE DS1006 processor board, following the guidelines given in [4]. The stator currents and the DC-link voltage are sampled in the beginning of each PWM period; both the switching and sampling frequencies are 5 kHz. The inverter nonlinearities are compensated for using a simple current feedforward method. The actual rotor speed is measured using an incremental encoder only for monitoring purposes. The control scheme shown in Fig. 1(a) was augmented with a speed controller (having the bandwidth of $2\pi \cdot 2$ rad/s), which provides the torque reference based on the speed reference and the estimated speed. The current controller has the bandwidth of $2\pi \cdot 200$ rad/s. For simplicity, the d-axis current reference $i_{\mathrm{d,ref}} = 0$ is applied. Thus, the q-axis current reference is $i_{\mathrm{q,ref}} = 2T_{\mathrm{ref}}/(3p\hat{\psi}_{\mathrm{f}})$.

B. Dynamic Performance

Fig. 4(a) shows the simulated response of PM-flux adaptation in a no-load condition at the speed of 750 r/min. PM-flux adaptation is enabled at $t = 0.01$ s. As predicted by the linearized model, PM-flux adaptation affects speed adaptation. Fig. 4(b) shows the corresponding experimental results, which match very well with the simulation results. The rise time of the PM-flux estimate from 10% to 90% is approximately 45 ms, which agrees very closely with the designed approximate bandwidth $a = 2\pi \cdot 7.5$ rad/s.

C. Sensitivity to Parameter Errors

Fig. 5 demonstrates the sensitivity of the observer to the PM-flux error. The motor is first accelerated to half the rated speed, and a 10-Nm load-torque step is applied at $t = 2.6$ s. Initial value of the PM-flux estimate is $\hat{\psi}_{\mathrm{f}}(0) = 0.49$ Vs and the actual value is $\psi_{\mathrm{f}} = 0.57$ Vs (the error is 15%). The actual value is obtained from a separate test, where the no-load back-EMF voltage is measured at half the rated speed. PM-flux adaptation is enabled at $t = 4$ s. It can be seen from Fig. 5 that the PM-flux estimate converges rapidly to the actual value and, simultaneously, the position-estimation error disappears.

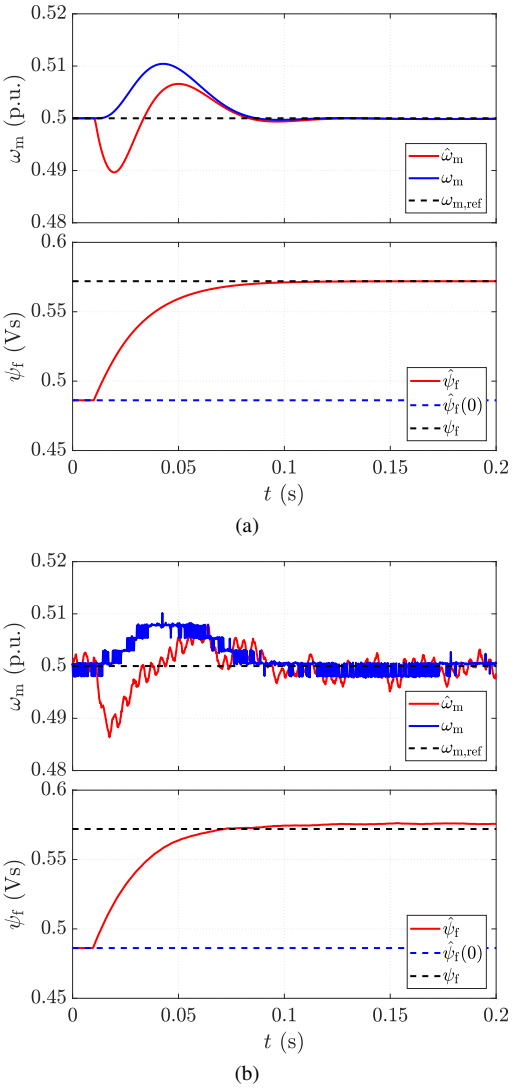

Fig. 4. Dynamic response of PM-flux adaptation: (a) simulation results; (b) experimental results. First subplot: estimated speed, actual speed, and speed reference. Second subplot: PM-flux estimate, its initial value, and actual PM flux.

Fig. 6 shows the sensitivity of the observer to the stator-resistance error. The motor is operating at the speed of 375 r/min and PM-flux adaptation is enabled throughout the sequence. The resistance estimate is erroneous between $t = 1$ and $t = 5$ s. Moreover, a 10-Nm load-torque step is applied at $t = 3$ s. It can be seen that the PM-flux estimate becomes inaccurate at this lower speed, if the resistance estimate is erroneous while the load torque is applied. Similar test sequences were applied to test the sensitivity to the inductance errors. According to the results, the observer is sensitive mostly to the errors in L_{q} and R.

VII. Conclusions

A back-EMF-based observer with PM-flux adaptation for motion-sensorless synchronous motor drives is proposed. A

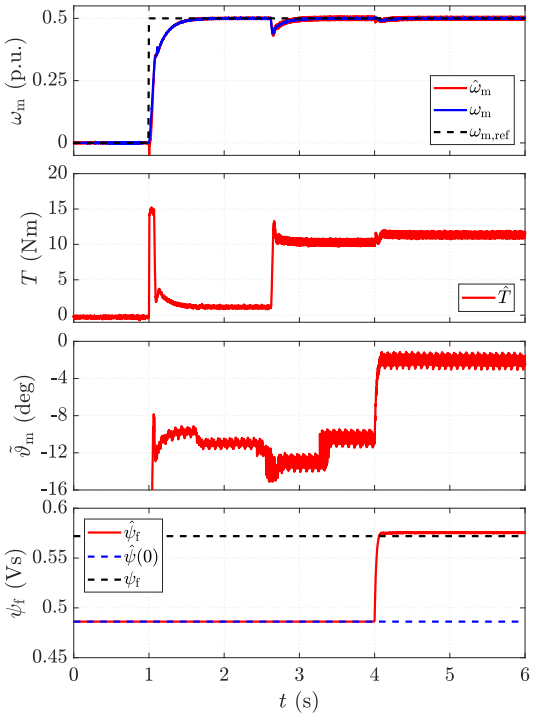

Fig. 5. Experimental results showing the effect of the PM-flux error. PM-flux adaptation is enabled at $t = 4$ s. First subplot: estimated speed, actual speed, and speed reference. Second subplot: estimated torque. Third subplot: angle-estimation error. Last subplot: PM-flux estimate, its initial value, and actual PM flux.

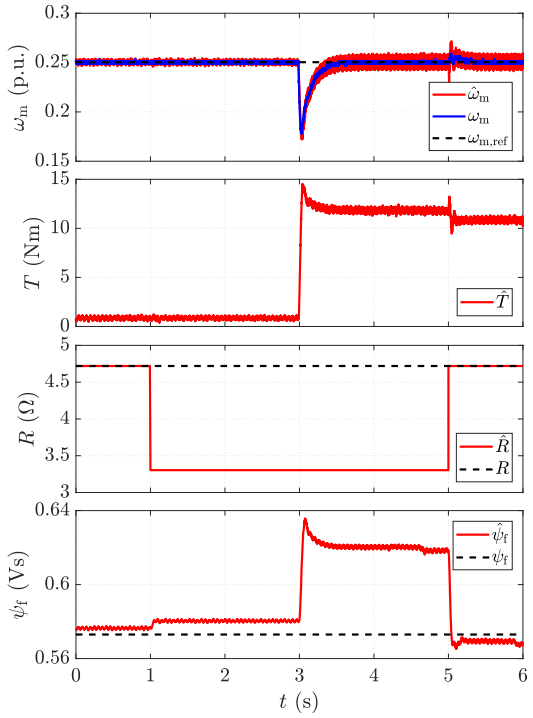

Fig. 6. Experimental results showing the sensitivity of the method to the resistance estimate. First subplot: estimated speed, actual speed, and speed reference. Second subplot: estimated torque. Third subplot: resistance estimate used in the control system and actual resistance. Last subplot: PM-flux estimate and actual PM flux.

gain selection is proposed for the augmented observer based on the linearized model. The proposed gain selection makes PM-flux estimation independent of speed estimation and enables straightforward analytical pole placement of the observer. Based on the simulation and experimental results, fast and accurate estimation of the PM flux can be obtained.

References

[1] S. Koonlaboon and S. Sangwongwanich, "Sensorless control of interior permanent-magnet synchronous motors based on a fictitious permanent-magnet flux model," in *Conf. Rec. IEEE-IAS Annu. Meeting*, Hong Kong, Oct. 2005, pp. 1111–1118.

[2] S. Sangwongwanich, S. Suwankawin, S. Po-ngam, and S. Koonlaboon, "A unified speed estimation design framework for sensorless ac motor drives based on positive-real property," in *Proc. PCC-Nagoya'07*, Nagoya, Japan, Apr. 2007, pp. 1111–1118.

[3] J. Lee, J. Hong, K. Nam, R. Ortega, L. Praly, and A. Astolfi, "Sensorless control of surface-mount permanent-magnet synchronous motors based on a nonlinear observer," *IEEE Trans. Power Electron.*, vol. 25, no. 2, pp. 290–297, Feb. 2010.

[4] M. Hinkkanen, S. E. Saarakkala, H. A. A. Awan, E. Mölsä, and T. Tuovinen, "Observers for sensorless synchronous motor drives: Framework for design and analysis," *IEEE Trans. Ind. Appl.*, 2018, early access.

[5] S. Odhano, R. Bojoi, S. Rosu, and A. Tenconi, "Identification of the magnetic model of permanent-magnet synchronous machines using DC-biased low-frequency AC signal injection," *IEEE Trans. Ind. Appl.*, vol. 51, no. 4, pp. 3208–3215, July 2015.

[6] N. Bedetti, S. Calligaro, and R. Petrella, "Stand-still self-identification of flux characteristics for synchronous reluctance machines using novel saturation approximating function and multiple linear regression," *IEEE Trans. Ind. Appl.*, vol. 52, no. 4, pp. 3083–3092, July/Aug. 2016.

[7] T. Sebastian, "Temperature effects on torque production and efficiency of PM motors using NdFeB magnets," *IEEE Trans. Ind. Appl.*, vol. 31, no. 2, pp. 353–357, Mar./Apr. 1995.

[8] K. Liu, Q. Zhang, J. Chen, Z. Q. Zhu, and J. Zhang, "Online multiparameter estimation of nonsalient-pole PM synchronous machines with temperature variation tracking," *IEEE Trans. Ind. Electron.*, vol. 58, no. 5, pp. 1776–1788, May 2011.

[9] D. Reigosa, D. Fernandez, T. Tanimoto, T. Kato, and F. Briz, "Comparative analysis of BEMF and pulsating high-frequency current injection methods for PM temperature estimation in PMSMs," *IEEE Trans. Power Electron.*, vol. 32, no. 5, pp. 3691–3699, May 2017.

[10] M. Hinkkanen, T. Tuovinen, L. Harnefors, and J. Luomi, "A combined position and stator-resistance observer for salient PMSM drives: design and stability analysis," *IEEE Trans. Power Electron.*, vol. 27, no. 2, pp. 601–609, Feb. 2012.

[11] K.-W. Lee, D.-H. Jung, and I.-J. Ha, "An online identification method for both stator resistance and back-EMF coefficient of PMSMs without rotational transducers," *IEEE Trans. Ind. Electron.*, vol. 51, no. 2, pp. 507–510, Apr. 2004.

[12] S. Ichikawa, M. Tomita, S. Doki, and S. Okuma, "Sensorless control of permanent-magnet synchronous motors using online parameter identification based on system identification theory," *IEEE Trans. Ind. Electron.*, vol. 53, no. 2, pp. 363–372, Apr. 2006.

[13] S. Morimoto, M. Sanada, and Y. Takeda, "Mechanical sensorless drives of ipmsm with online parameter identification," *IEEE Trans. Ind. Appl.*, vol. 42, no. 5, pp. 1241–1248, Sept./Oct. 2006.

[14] A. Piippo, M. Hinkkanen, and J. Luomi, "Adaptation of motor parameters in sensorless PMSM drives," *IEEE Trans. Ind. Appl.*, vol. 45, no. 1, pp. 203–212, Jan./Feb. 2009.

[15] T. Tuovinen and M. Hinkkanen, "Signal-injection-assisted full-order observer with parameter adaptation for synchronous reluctance motor drives," *IEEE Trans. Ind. Appl.*, vol. 50, no. 5, pp. 3392–3402, Sept./Oct. 2014.

[16] T. Tuovinen, M. Hinkkanen, L. Harnefors, and J. Luomi, "Comparison of a reduced-order observer and a full-order observer for sensorless synchronous motor drives," *IEEE Trans. Ind. Appl.*, vol. 48, no. 6, pp. 1959–1967, Nov./Dec. 2012.